Coupled Vortex Oscillations in Spatially Separated Permalloy Squares

Andreas Vogel, Thomas Kamionka, Michael Martens, André Drews, Kang Wei Chou, Tolek Tyliszczak, Hermann Stoll, Bartel Van Waeyenberge, and Guido Meier

Phys. Rev. Lett. **106**, 137201 — Published 29 March 2011

DOI: 10.1103/PhysRevLett.106.137201

Coupled vortex oscillations in spatially separated permalloy squares

Andreas Vogel,[1,*] Thomas Kamionka,[1] Michael Martens,[1] André Drews,[1,2] Kang Wei Chou,[3] Tolek Tyliszczak,[3] Hermann Stoll,[4] Bartel Van Waeyenberge,[5] and Guido Meier[1]

[1]*Institut für Angewandte Physik und Zentrum für Mikrostrukturforschung, Universität Hamburg, 20355 Hamburg, Germany*

[2]*Arbeitsbereich Technische Informatik Systeme, Universität Hamburg, 22527 Hamburg, Germany*

[3]*Advanced Light Source, Lawrence Berkeley National Laboratory, Berkeley, 94720 California, USA*

[4]*Max-Planck-Institut für Metallforschung, 70569 Stuttgart, Germany*

[5]*Department of Solid State Sciences, Ghent University, 9000 Ghent, Belgium*

Abstract

We experimentally study the magnetization dynamics of pairs of micron-sized permalloy squares coupled via their stray fields. The trajectories of the vortex cores in the Landau-domain patterns of the squares are mapped in real space using time-resolved scanning transmission X-ray microscopy. After excitation of one of the vortex cores with a short magnetic-field pulse, the system behaves like coupled harmonic oscillators. The coupling strength depends on the separation between the squares and the configuration of the vortex-core polarizations. Considering the excitation via a rotating in-plane magnetic field, it can be understood that only a weak response of the second vortex core is observed for equal core polarizations.

PACS numbers: 75.70.Kw, 03.65.Ge, 68.37.Yz

Sub-nanosecond dynamics and potential technological applications, e.g., in ultra-fast and high-density digital storage devices or microwave emission sources give rise to a broad scientific interest in the dynamic properties of ferromagnetic microstructures with vortex magnetization configuration [1–7]. Vortices appear in ferromagnetic thin-film squares where a magnetization configuration with magnetic moments pointing in-plane and parallel to the edges is energetically favorable. In the center, the short-range exchange coupling which favors a parallel orientation of the magnetic moments forces the magnetization out-of-plane. Vortex configurations are characterized by their polarization $p = \pm 1$ and their chirality $C = \pm 1$ describing the magnetization orientation of the core and the in-plane counterclockwise or clockwise curling of the magnetization around the core, respectively. Once deflected and released, vortices exhibit a spiral motion around their equilibrium position where the sense of gyration depends on the polarization p. For small deflections, the trajectory can be described analytically as a two-dimensional harmonic oscillator [8].

The magnetostatic interaction between spatially separated structures has to be taken into account when the inter-element distance is smaller than the lateral size of the elements [9]. Previous studies focus on the dynamics of interacting vortices that are excited simultaneously [10–12]. In arrays of ferromagnetic disks, the resonance frequency of the vortex-core motion is strongly affected [13, 14]. However, dynamic interaction with individual elements has to be further investigated [15, 16]. For many applications, a high packing density is desired and the stray-field mediated interaction is important, e.g., with respect to cross talk in potential memory devices. Only recently, it has been shown experimentally that vortex gyrations can be induced by dipolar interaction between physically disconnected ferromagnetic disks [17].

We experimentally demonstrate coupled vortex gyrations in pairs of spatially separated permalloy squares. The core trajectories are determined by time-resolved X-ray microscopy. After exciting one element via a short magnetic-field pulse in the plane of the square, the stray field of the excited structure induces a gyration of the vortex in the adjacent square. An oscillatory change of the gyration amplitudes in the two squares is observed. The interacting vortices reveal a fundamental behavior known from other coupled harmonic oscillators. Distinct normal modes for in-phase and antiphase motion of the vortex cores can be identified. The coupling strength depends on the separation distance between the squares and the configuration of the core polarizations.

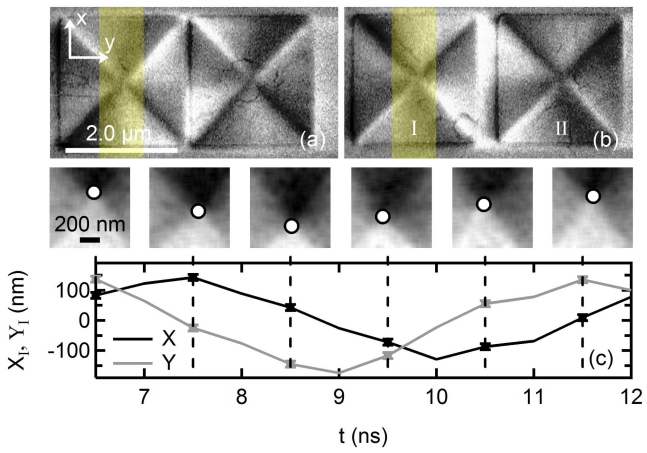

FIG. 1: (Color online) Magnetic force micrographs of two pairs of permalloy squares with a center-to-center distance of (a) $d = 2.25$ μm and (b) $d = 2.5$ μm. A stripline (illustrated in yellow) is deposited on top of the left square (I). (c) X-ray images showing the time-dependent in-plane magnetic contrast in the center part of square I after excitation at zero-time. Here, the time step between two successive images is 1.0 ns. White dots designate the position of the vortex core. Black and gray lines in the graph mark the evaluated deflection in x- and y-direction, respectively. The x-axis is corrected according to the tilt of the sample.

Pairs of ferromagnetic squares as shown in Fig. 1(a) and 1(b) are fabricated using electron-beam lithography and lift-off processing. Polycrystalline permalloy ($Ni_{80}Fe_{20}$) with a thickness of 60 nm is thermally evaporated onto a 100 nm thin silicon-nitride membrane. The edge length of the squares is $l = 2.0$ μm and the center-to-center distance d is varied from 2.25 μm to 3.5 μm. Magnetic force micrographs confirm the presence of Landau-domain patterns with a single vortex core. A 800 nm wide stripline of 150 nm copper and a gold cap of a few nanometers is deposited on top of the left squares (I) via thermal evaporation, illustrated in Fig.1.

The measurements have been performed using time-resolved scanning transmission X-ray microscopy (STXM) [18] at beamline 11.0.2 of the Advanced Light Source (ALS) in Berkeley, CA, USA. Magnetic contrast is provided via the X-ray magnetic circular dichroism (XMCD) at the Ni L_3-absorption edge (852.7 eV) [19]. Images are taken in a configuration sensitive to the in-plane magnetization with the sample mounted under an angle of 60° and in a configuration sensitive to the out-of-plane magnetization with the sample mounted perpendicular to the beam axis. The latter configuration enables to directly image the magnetization of the

vortex core and the core trajectory is mapped with significantly higher precision. A current pulse of 1.8 ns duration through the stripline initially deflects the vortex core in element I via the resulting magnetic-field pulse of ≈ 3 mT in the plane of the square. The magnetic response is detected in time steps of 500 ps. Figure 1(c) shows the time-dependent in-plane magnetic contrast of a square located under the stripline. The deflection $\mathbf{X}_{\mathrm{I}} = (X_{\mathrm{I}}, Y_{\mathrm{I}})$ in x- and y-direction is determined from the X-ray images. The period of 5.5 ns corresponds to a frequency of 182 MHz which is in accordance with the eigenfrequency of vortex gyration in single elements [20].

Figures 2(a) and 2(b) show the time-dependent trajectories of two different pairs determined from X-ray images after excitation of element I. The two elements I under the stripline [solid and dashed lines in Fig. 2(a)] have opposite core polarizations p and opposite chiralities C which leads to an in-phase motion in x- and an antiphase motion in y-direction. Note that opposite chiralities lead to an initial deflection in the opposite direction of the y-axis. Figure 2(b) unambiguously reveals magnetization dynamics in the elements II next to the stripline which proves the coupling via the stray fields. For these elements, the Oersted field of the stripline is not the main source of excitation since there is a considerable time-delay of more than 10 ns in the maximum amplitude between the two elements I and II. The elements represented by the solid lines in Figs. 2(a) and 2(b) have opposite polarizations and same chiralities which leads to an in-phase motion in x- and an antiphase motion in y-direction. Since the elements represented by the dashed lines have opposite polarizations and opposite chiralities, an antiphase motion in x- and an in-phase motion in y-direction is observed. There is no significant difference in the maximum displacements $|\mathbf{X}_{\mathrm{IImax}}|$ between the two cases which indicates that the chirality does not play an important role for the coupling strength. It just leads to a phase shift.

Figure 2(c) reveals only weak motion of the vortex core in element II in the case of same core polarizations ($p_{\mathrm{I}} = p_{\mathrm{II}}$). The gyration amplitude in element I decreases exponentially which corresponds to the behavior of a single element. Fitting the time-dependent displacement $|\mathbf{X}_{\mathrm{I}}|$ with an exponential function yields a damping parameter $\Gamma = (2.98 \pm 0.10) \times 10^7$ s^{-1}. The parameter Γ depends on the gyration frequency, the sample geometry and the Gilbert damping parameter α [8]. A gyration of the vortex core in element I leads to a time-dependent change of the local stray field. To get an idea of this stray field, micromagnetic simulations of a square with a thickness of 20 nm and an

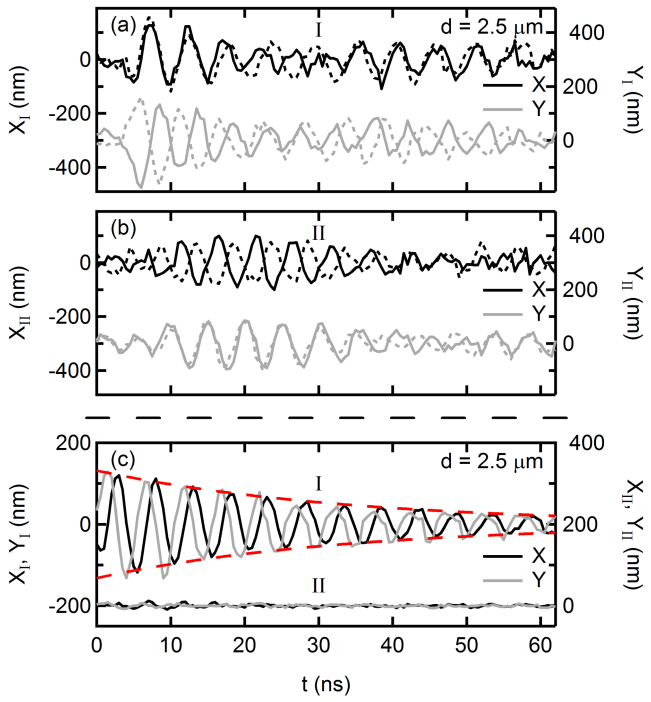

FIG. 2: (Color online) Trajectories of vortex cores after pulse excitation in three pairs of ferromagnetic squares ($d = 2.5$ μm) with different chirality and polarization configurations determined with (a), (b) in-plane and (c) out-of-plane magnetic contrast. Black and gray lines mark the deflection in x- and y-direction, respectively. For opposite core polarizations ($p_{\mathrm{I}} = -p_{\mathrm{II}}$), the deflections X_{I}, Y_{I} of the vortex in the elements I are shown in (a) and the deflections X_{II}, Y_{II} in the elements II are shown in (b). Pairs with different chirality configuration are marked as solid ($C_{\mathrm{I}} = C_{\mathrm{II}}$) and dashed ($C_{\mathrm{I}} = -C_{\mathrm{II}}$) lines. For same core polarizations ($p_{\mathrm{I}} = p_{\mathrm{II}}$), the deflections X_{I}, Y_{I}, X_{II} and Y_{II} for one pair are shown in (c). The dashed red lines illustrate the exponential decrease of $|\mathbf{X}_{\mathrm{I}}|$. Core positions can be determined with an accuracy of ± 10 nm for the in-plane and ± 5 nm for the out-of-plane configuration. STXM measurements are available as movies S1 and S2 in the supplementary material [21].

edge length of $l = 200$ nm [22] are performed using the Object Oriented MicroMagnetic Framework (OOMMF) [23] with a cell size of $2 \times 2 \times 20$ nm^3. A saturation magnetization $M_s = 8 \times 10^5$ A/m, an exchange constant $A = 13 \times 10^{-12}$ J/m, and $\alpha = 0.01$ are assumed. In the vortex ground state, a fourfold symmetry is observed, see Fig. 3(a). Figure 3(b) reveals that the symmetry of the stray field is broken for an off-centered vortex core. However, at a sufficiently large distance from the square, the shape of the stray field reminds of the field

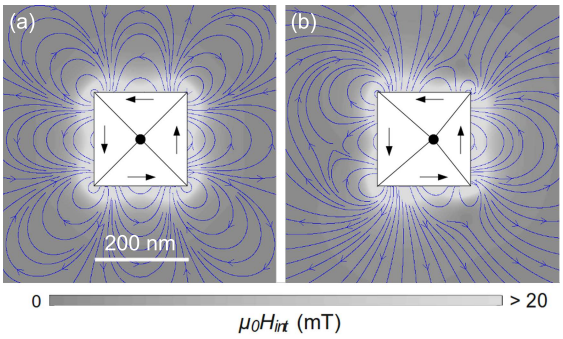

FIG. 3: (Color online) Micromagnetic simulations of the stray field $\mathbf{H}_{int}$ of a square (a) in the vortex ground state and (b) with an off-centered vortex core (black circle). Arrows outside the squares represent streamlines of the stray field. Arrows inside the squares indicate the direction of the magnetization in the domains ($C = 1$).

of a dipole located in the center of the square. In the case of $p_{\rm I} = p_{\rm II}$, the sense of rotation of the stray field opposes the intrinsic sense of gyration of the vortex core in element II. It has been shown that an in-plane rotating field only efficiently excites the gyrotropic mode when the sense of rotation of the field coincides with the sense of gyration given by the core polarization [24, 25]. The stray field of a square is not rotationally symmetric, compare Fig. 3(b). However, this analogy helps to understand the significant difference between the two polarization configurations.

For small deflections, the sum of the exchange energy and the self-magnetostatic energy of a single off-centered vortex core can be expanded in a series on the displacement $|\mathbf{X}_i|$. This energy contribution can be written as $(\kappa/2)\,(X_i^2 + Y_i^2)$, where the stiffness constant κ is a function of the geometry and the material parameters of the ferromagnetic square [8, 10, 13]. Assuming a rigid vortex core, the equation of motion [26] describes two-dimensional weakly damped harmonic oscillations in a parabolic potential. Neighboring squares couple via their stray fields when the inter-element distance is below their lateral size [9–17]. The interaction gives rise to an additional energy term. Then the equation of motion describes two-dimensional weakly damped coupled oscillations of the pair (I, II). Two normal modes arise in a pair of two weakly interacting oscillators - a low-frequency mode (ω_1) with an in-phase and a high-frequency mode (ω_2) with an antiphase movement of the oscillators. Any other motion of the coupled system can be described as a superposition of these two normal modes. For each of the two polarization configurations ($p_{\rm I} = p_{\rm II}$ or $p_{\rm I} = -p_{\rm II}$), two

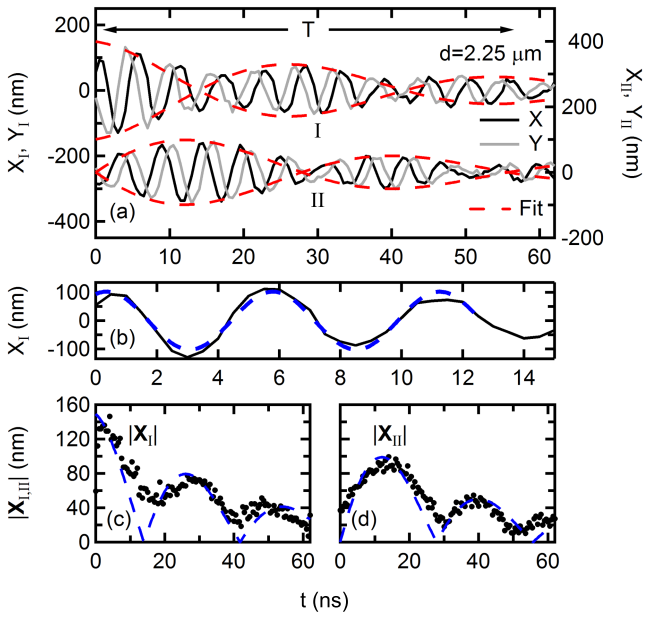

FIG. 4: (Color online) (a) Time-dependent deflections of the vortex cores in a pair with $p_{\mathrm{I}} = -p_{\mathrm{II}}$ and $d = 2.25$ μm determined via STXM in out-of-plane configuration. Black and gray lines mark the deflection in x- and y-direction, respectively. The dashed red lines illustrate the beating. (b) Deflection X_{I} (black line) and displacements (c) $|\mathbf{X}_{\mathrm{I}}|$ and (d) $|\mathbf{X}_{\mathrm{II}}|$ (black dots) of the cores. Fits in (b)-(d) are shown as dashed blue lines.

different normal modes are expected to occur [10]. In the following, we concentrate on the experiments with opposite core polarizations.

Only one core is initially deflected and thus a superposition of the two normal modes - for in-phase (ω_1) and antiphase (ω_2) motion - is excited. The vortex cores gyrate with the angular frequency $\omega_+ = (\omega_1 + \omega_2)/2$. The amplitude of these gyrations is modulated with the beating frequency $\omega_- = (\omega_2 - \omega_1)/2$. This can be interpreted in terms of energy exchange between the two vortex cores [17]. Energy dissipation causes a time-dependent decrease of the displacements $|\mathbf{X}_{\mathrm{I}}|$ and $|\mathbf{X}_{\mathrm{II}}|$. Figure 4(a) exhibits a full beating period $T = 4\pi/(\omega_2 - \omega_1)$. A gyration frequency of $\omega_+/(2\pi) = (179 \pm 3)$ MHz is obtained by fitting the time-dependent deflections in x- and y-direction with a sinusoidal function, e.g., $X_{\mathrm{I}} = K \sin(\omega_+ t + \phi)$, see Fig. 4(b). In addition, the displacements of both vortex cores can be fitted with the two orthogonal exponentially damped sinusoidal functions $|\mathbf{X}_{\mathrm{I}}| = |D \cos(\omega_- t)| \exp(-\beta t)$ and $|\mathbf{X}_{\mathrm{II}}| = |E \sin(\omega_- t)| \exp(-\beta t)$. The fits shown in Figs. 4(c) and 4(d) yield a beating frequency $\omega_-/(2\pi) = (18 \pm 1)$ MHz and an energy

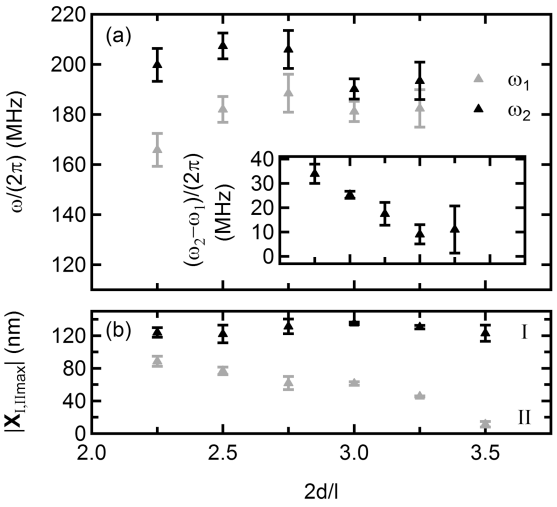

FIG. 5: (a) Normal mode frequencies ω_1 (gray) and ω_2 (black) in dependence on the normalized center-to-center distances $2d/l$. The inset shows the frequency splitting $\omega_2 - \omega_1$. (b) Maximum displacements $|\mathbf{X}_{\mathrm{Imax}}|$ (black) and $|\mathbf{X}_{\mathrm{IImax}}|$ (gray) of the vortex cores.

dissipation parameter $\beta = (2.39 \pm 0.06) \times 10^7$ s^{-1}. Taking into account the result for ω_+, the frequencies of the two normal modes are identified to be $\omega_1/(2\pi) = (161 \pm 3)$ MHz for in-phase and $\omega_2/(2\pi) = (197 \pm 3)$ MHz for antiphase motion. Note that $\beta \approx \Gamma$, compare Fig. 2(c), which indicates that the energy dissipation is mainly given by the material and the geometry of the single elements.

Figure 5(a) shows the two normal mode frequencies ω_1 and ω_2 in different pairs (I, II) as a function of the normalized center-to-center distance $2d/l$. The coupling strength decreases with increasing separation and thus the two normal modes approach each other. A decreasing frequency splitting $\omega_2 - \omega_1$ corresponds to an increase of the beating period. Due to the damping of the system, the average values of the maximum gyration amplitude $|\mathbf{X}_{\mathrm{IImax}}|$ in element II decrease with increasing separation, whereas the maximum amplitude in element I remains approximately the same. STXM measurements are available as movie S3 in the supplementary material [21]. No significant movement of the vortex core in element II could be observed for a normalized center-to-center distance of $2d/l = 3.5$ and thus the coupling can be neglected.

In summary, we have directly observed the stray-field coupled harmonic oscillations of vortices with opposite core polarizations in pairs of spatially separated permalloy squares. A superposition of the two normal modes for in-phase and antiphase motion has been ex-

cited via a short magnetic field pulse applied to one of the two elements. With increasing separation, the coupling within the pair is notably decreased. A dependence on the core polarization configuration can be understood by considering the excitation via a rotating in-plane magnetic field.

We thank Hyunsung Jung and Sang-Koog Kim for fruitful discussions, Ulrich Merkt for fruitful discussions and continuous support, Sebastian Wintz for providing some of his beamtime at the STXM, and Michael Volkmann for superb technical assistance. Financial support of the Deutsche Forschungsgemeinschaft via the Sonderforschungsbereich 668 and the Forschungs- und Wissenschaftsstiftung Hamburg via the Exzellenzcluster "Nano-Spintronik" is gratefully acknowledged. Operation of the X-ray microscope is supported by the DOE, Office of Science, under contract DE-AC02-05-CH11231.

* Electronic address: andreas.vogel@physnet.uni-hamburg.de

[1] T. Shinjo *et al.*, Science **289**, 930 (2000).

[2] R. P. Cowburn *et al.*, Phys. Rev. Lett. **83**, 1042 (1999).

[3] K. S. Buchanan *et al.*, Nat. Phys. **1**, 172 (2005).

[4] S.-K. Kim *et al.*, Appl. Phys. Lett **92**, 022509 (2008).

[5] S. Bohlens *et al.*, Appl. Phys. Lett. **93**, 142508 (2008).

[6] V. S. Pribiag *et al.*, Nat. Phys. **3**, 498 (2007).

[7] Q. Mistral *et al.*, Phys. Rev. Lett **100**, 257201 (2008).

[8] B. Krüger *et al.*, Phys. Rev. B **76**, 224426 (2007).

[9] V. Novosad *et al.*, Phys. Rev. B **65**, 060402(R) (2002).

[10] J. Shibata *et al.*, Phys. Rev. B **67**, 224404 (2003).

[11] Y. Liu *et al.*, Phys. Rev. B **79**, 104435 (2009).

[12] G. Gubbiotti *et al.*, J. Appl. Phys. **99**, 08C701 (2006).

[13] A. Vogel *et al.*, Phys. Rev. Lett. **105**, 037201 (2010).

[14] A. Barman *et al.*, J. Phys. D: Appl. Phys. **43**, 422001 (2010).

[15] S. Barman *et al.*, J. Phys. D: Appl. Phys. **43**, 335001 (2010).

[16] S. Sugimoto *et al.*, arXiv:1009.3363 (2010).

[17] H. Jung *et al.*, Appl. Phys. Lett. **97**, 222502 (2010); H. Jung *et al.*, arXiv:1011.6399 (2010).

[18] B. Van Waeyenberge *et al.*, Nature **444**, 461 (2006).

[19] C. T. Chen *et al.*, Phys. Rev. B **42**, 7262 (1990).

[20] V. Novosad *et al.*, Phys. Rev. B **72**, 024455 (2005).

[21] See supplementary material for movies S1, S2, and S3.

[22] A scaled-down square in micromagnetic simulations provides tractable computation times. The general nature of the stray field remains the same.

[23] http://math.nist.gov/oommf/.

[24] K.-S. Lee *et al.*, Phys. Rev. B **78**, 014405 (2008).

[25] M. Curcic *et al.*, Phys. Rev. Lett. **101**, 197204 (2008).

[26] A. A. Thiele, Phys. Rev. Lett. **30**, 230 (1973).